INTERNATIONAL JOURNAL FOR NUMERICAL METHODS IN ENGINEERING
Int. J. Numer. Meth. Engng 2004; **61**:2114–2138
Published online 18 October 2004 in Wiley InterScience (www.interscience.wiley.com). DOI: 10.1002/nme.1152

Supersensitivity due to uncertain boundary conditions[‡]

Dongbin Xiu and George Em Karniadakis[*, †]

Division of Applied Mathematics, Box F, Brown University, Providence, RI 02912, U.S.A.

SUMMARY

We study the viscous Burgers' equation subject to perturbations on the boundary conditions. Two kinds of perturbations are considered: deterministic and random. For deterministic perturbations, we show that small perturbations can result in $O(1)$ changes in the location of the transition layer. For random perturbations, we solve the stochastic Burgers' equation using different approaches. First, we employ the Jacobi-polynomial-chaos, which is a subset of the generalized polynomial chaos for stochastic modeling. Converged numerical results are reported (up to seven significant digits), and we observe similar 'stochastic supersensitivity' for the mean location of the transition layer. Subsequently, we employ up to fourth-order perturbation expansions. We show that even with small random inputs, the resolution of the perturbation method is relatively poor due to the larger stochastic responses in the output. Two types of distributions are considered: uniform distribution and a 'truncated' Gaussian distribution with no tails. Various solution statistics, including the spatial evolution of probability density function at steady state, are studied. Copyright © 2004 John Wiley & Sons, Ltd.

KEY WORDS: generalized polynomial chaos; stochastic Burgers' equation; supersensitivity; random boundary conditions

1. INTRODUCTION

We consider the viscous Burgers' equation,

$$\begin{aligned} u_t + uu_x &= \nu u_{xx}, \quad x \in [-1, 1] \\ u(-1) &= 1 + \delta, \quad u(1) = -1 \end{aligned} \tag{1}$$

where $\delta > 0$ is a small perturbation to the left boundary condition ($x = -1$) and $\nu > 0$ is the viscosity. The presence of viscosity smoothes out the shock discontinuity which will develop otherwise. Thus, the solution has a transition layer, which is a region of rapid variation and

[*]Correspondence to: G. Karniadakis, Division of Applied Mathematics, Box F, Brown University, Providence, RI 02912, U.S.A.
[†]E-mail: gk@cfm.brown.edu
[‡]This work was supported by DOE, NSF, and AFOSR.

Contract/grant sponsor: DOE, NSF and AFOSR

Received 18 February 2004
Revised 19 May 2004
Accepted 28 May 2004

extends over a distance $O(\nu)$ as $\nu \downarrow 0$. The location of the transition layer z, defined as the zero of the solution profile $u(z) = 0$, varies with time, and its eventual location at steady state is extremely sensitive to the boundary data. This phenomenon, termed *supersensitivity* in *deterministic* asymptotic analysis, was first observed by Lorentz [1]. In this paper, we will present numerical solutions that exhibit supersensitivity under both deterministic and random perturbations on the boundary condition. In particular, we consider the following two cases:

1. $0 < \delta \ll O(1)$ is a deterministic value;
2. $\delta \in (0, \varepsilon)$ is a random variable in $(0, \varepsilon)$ with $\varepsilon \ll O(1)$ and a given continuous probability distribution function (PDF) $f(\delta)$.

For problems with deterministic perturbations, extensive research efforts by asymptotic analysis have been devoted to the Burgers' equation and more general viscous conservation laws in one spatial dimension (see References [2–8]). In Reference [9], numerical simulations were conducted for both one-dimensional Burgers' equation and its two-dimensional generalization. The results agree well with the asymptotic estimates. In the first part of this paper, we revisit the deterministic supersensitivity problem via two numerical approaches. First, we solve the exact formula at steady state. This formula defines the steady state solution implicitly in a non-linear way. Although it has been known in the literature, its solution has rarely been sought. Here we solve it iteratively with high accuracy for some chosen parameters. Subsequently, we conduct direct numerical simulations by integrating the Burgers' equation (1) via the spectral/hp element method [10]. It is shown that the results from the direct simulations agree with the exact solution for up to seven significant digits. In a previous work we have reported preliminary results that showed similar *stochastic supersensitivity* when the perturbation δ on the boundary condition is random [11]. In the current work, we extend these results and present more systematic studies. We also note that uncertainty quantification in boundary conditions for incompressible Navier–Stokes equations, for both random variables as well as random processes, has been studied in References [12–14].

For stochastic partial differential equations,existing techniques can be broadly classified into two categories: methods using a statistical approach and methods using a non-statistical approach. The statistical approach includes Monte Carlo simulation, stratified sampling, Latin hypercube sampling, etc. These methods involve sampling and estimation and their accuracy depend on the sample size, in accordance with the 'weak law of large number'. Therefore, simulations can be prohibitively expensive, especially for the systems that are already complicated in the *deterministic* case. Thus, more research effort has been devoted to developing non-statistical methods. The most popular non-statistical method is the perturbation method, where the random field is expanded via Taylor series around its mean and truncated at certain order. Typically, at most second-order expansion is employed because the system of equations becomes increasingly complicated beyond second-order. This approach, also called the 'second moment analysis' [15–17], has been used extensively in various fields [18–25]. The limitation of the perturbation method is that the uncertainties cannot be too large. Typically, the standard deviations of the random quantities need to be less than 10% compared to their mean values [16].

Another methodology of the non-statistical type is to 'expand'random fields directly. A framework of representing random fields by orthogonal polynomial functionals, called the *generalized polynomial chaos*, was proposed in Reference [26]. It is a generalization of the original Hermite polynomial chaos theory by Wiener [27], which has been applied to various problems by Ghanem *et al*. (see [12, 13, 28–32], etc). Also, some work has been done to combine

the Wiener–Hermite polynomial chaos with Monte Carlo methods to design efficient algorithms [33, 29]. Other work concerning various properties, including the limitations of Wiener–Hermite expansions, can be found in References [34–38]. The *generalized polynomial chaos* expansion is essentially a spectral expansion of random variables, and employs a wider class of orthogonal polynomials than Hermite polynomials from the Askey scheme to represent stochastic processes more efficiently. (Detailed account of Askey scheme and their connections to stochastic processes can be found in References [39, 40].) It has been applied to applications of stochastic ODE, elliptic equation, fluid dynamics, etc. ([14, 26, 41, 42]). Its convergence and efficiency, especially the exponential convergence under ideal conditions, is demonstrated in these applications. An analysis on the well-posedness of the discrete system of the chaos expansion for diffusion problems reveals that the Jacobi polynomial chaos is more flexible than the others [43]. Also, recently a theoretical framework for discretizing random fields via the finite element approach, i.e. piecewise polynomials, was proposed in References [44–46]. For an overview of the general mathematical challenges in solving stochastic partial differential equations, see References [47–49]. For studies on the general aspects of Burgers' equation subject to uncertain inputs, see References [50, 51].

In this paper, we apply the generalized polynomial chaos expansion to the Burgers' equation (1) with random perturbation on the boundary condition. In particular, since the random input is assumed to have bounded support, we employ the corresponding Jacobi polynomial chaos. Resolution refinement studies, both in physical and random spaces, are conducted, and we present numerical results converged to seven significant digits. On the other hand, a perturbation method is also employed and we use as high as fourth-order expansion. The results, however, are relatively poor, and they do not improve as the order of the perturbation expansion increases.

The remaining part of the paper is organized as follows. In Section 2, we study the deterministic supersensitivity problem. We review briefly the asymptotic analysis results and present high resolution numerical results both from an exact formula and from direct integration of Burgers' equation (1) by the spectral/hp element method. In Section 3, the stochastic supersensitivity is considered, and we present the formulations for the stochastic Burgers' equation by generalized polynomial chaos and perturbation method. Detailed numerical studies are presented in Section 4 and we conclude the paper with a brief summary in Section 5. Technical details are included in Appendices A–C.

2. DETERMINISTIC SUPERSENSITIVITY

In this section, we study the viscous Burgers' equation (1) with a small *deterministic* perturbation $\delta > 0$ on the upstream boundary condition.

2.1. Exact solution

The viscous Burgers' equation (1) has an exact solution at steady state

$$u(x) = -A \tanh\left[\frac{A}{2\nu}(x - z_{\text{ex}})\right] \tag{2}$$

where z_{ex} is the location of transition layer where $u(z_{\text{ex}}) = 0$ and $-A = \partial u/\partial x|_{x=z_{\text{ex}}}$ is its slope at this location. These two unknowns are determined by the two boundary

conditions

$$A \tanh\left[\frac{A}{2v}(1+z_{\text{ex}})\right] = 1+\delta, \quad A \tanh\left[\frac{A}{2v}(1-z_{\text{ex}})\right] = 1 \tag{3}$$

We can eliminate z_{ex} and obtain a single equation for A

$$(1+\delta+A^2)\tanh(A/v) = (2+\delta)A \tag{4}$$

Thus, we can solve (4) for A first and then solve z_{ex} from one of the equations in (3). Iterative methods are needed for these non-linear equations. It should be noted that the convergence is very sensitive to the choices of initial guess due to the 'supersensitive' nature of the original problem.

2.2. Asymptotic analysis

There has been a great number of publications on the asymptotic analysis of the supersensitivity of Burgers' equation and other viscous conservation laws, see References [2–8] and the references therein. Here we briefly summarize the results for Burgers' equation (1). Based on the asymptotic expansions of (2) and (3), it can be shown that if the viscosity v is small and δ satisfies

$$\delta = O(\mathrm{e}^{-a/v}) \quad \text{as } \delta, v \downarrow 0 \tag{5}$$

for some constant $a \in (0, 1)$ which does not depend on δ or v, then the position of the transition layer, defined as the zero of the solution profile $u(z) = 0$, varies on a transcendentally slow time scale

$$t^* = t\mathrm{e}^{-a/v} \tag{6}$$

The limit of the transition layer position at steady state is

$$z_{\text{as}} = 1 + v\ln(\delta/2), \quad t^* \to \infty \tag{7}$$

The asymptotic relation (5) implies that δ is transcendentally small (in the sense of asymptotic analysis) compared to v, but dominates $\mathrm{e}^{-1/v}$ as $v \downarrow 0$. Equation (7) shows that this transcendentally small perturbation δ leads to a measurable, i.e. order one, effect on the final location of the transition layer. This phenomenon is called *supersensitivity*.

2.3. Direct numerical simulations

Although numerical solutions can be obtained by solving the exact solutions (2) and (3), it is non-trivial to construct robust initial conditions that guarantee convergence of the iterative solvers in the parameter range of supersensitivity. Hence we seek high accurate numerical solutions by integrating Burgers' equation (1) directly. Equation (1) is integrated by the semi-implicit scheme. Since we are only interested in the steady state solution, a first-order scheme is employed

$$\frac{u^{n+1}-u^n}{\Delta t} + (uu_x)^n = vu_{xx}^{n+1} \tag{8}$$

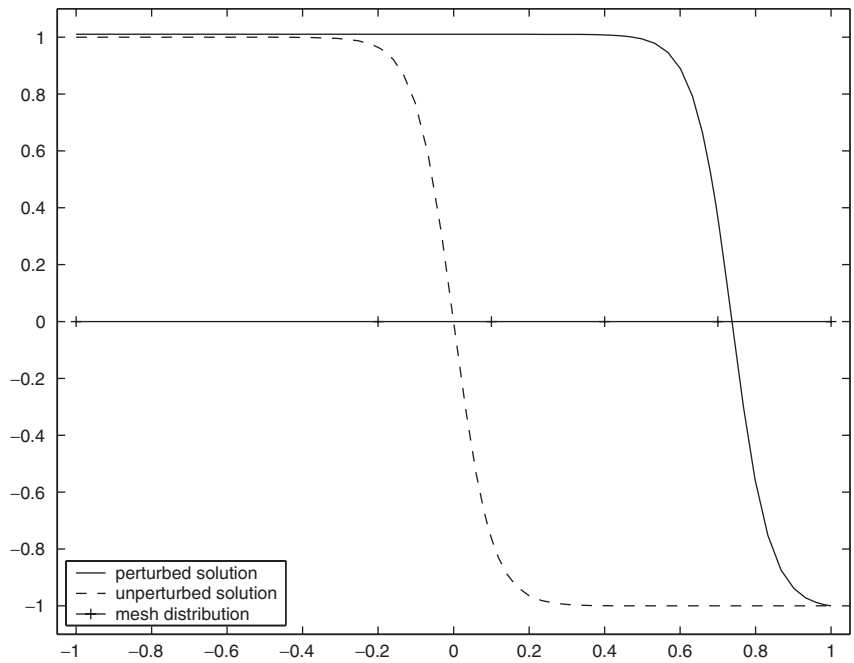

Figure 1. Schematic of the deterministic supersensitivity computation ($v = 0.05$). Solid line denotes the perturbed solution ($\delta = 0.01$); dashed line denotes the unperturbed solution ($\delta = 0$) which is centred at $x = 0$. Also shown is the distribution of the five non-uniform elements.

where the superscript n denotes the time level $t^n = n\Delta t$. However, high resolution is required in space in order to capture accurately the location of the transition layer, which is 'supersensitive' to the small perturbation on the boundary condition.

Garbey and Kaper [9], used a domain decomposition method with two non-overlapping subdomains, where the interface is adaptively located near the position of the transition layer. The Chebychev collocation method is employed and they found that with $N = 39$ collocation points in each subdomain the computed location of transition layer converges with three significant digits.

In this work we employ the spectral/hp element method that combines the high accuracy of traditional spectral methods and the flexibility of mesh control from finite element methods [10]. Improved solution can be obtained by either redistributing the elements non-uniformly across the computational domain (h-refinement) or increasing the order of polynomials within each element (p-refinement), or both (hp-refinement). Thus, spectral element methods offer a dual-path of convergence. Here we employ the modal-basis, continuous-Galerkin method, where Jacobi polynomials are used as the basis polynomials within elements (see Reference [10] for details).

In Figure 1, the steady state solution of (1) with $v = 0.05$ is shown. The solid line is the perturbed solution with $\delta = 0.01$, and the unperturbed solution with $\delta = 0$ is shown in dashed line for reference. Also shown in the figure is the distribution of five elements. The first element occupies $(-1, -0.2)$ and the rest divide the interval $(-0.2, 1)$ equally. Smaller mesh

Table I. Locations of transition layer of Burgers' equation with $\nu = 0.1$ subject to deterministic perturbation on boundary condition.

δ	z_{as}	z_{GK}	z	z_{ex}
10^{-1}	0.700427	0.72464	0.72322525	0.72322525
10^{-2}	0.470176	0.47486	0.47492742	0.47492741
10^{-3}	0.240724	0.24133	0.24142361	0.24142361
10^{-4}	0.052606	0.05265	0.052669616	0.052669612
10^{-5}	0.005504	0.00537	0.0055085545	0.0055085559

z_{as} is the asymptotic estimate from (7), z_{GK} is the numerical result from [9], z is the present direct numerical computation, and z_{ex} is the numerical solution from exact formula (3).

Table II. Locations of transition layer of Burgers' equation with $\nu = 0.05$ subject to deterministic perturbation on boundary condition.

δ	z_{as}	z_{GK}	z	z_{ex}
10^{-1}	0.850213	0.86237	0.86161262	0.86161262
10^{-2}	0.735084	0.73755	0.73746015	0.73746015
10^{-3}	0.619955	0.62055	0.62030957	0.62030957
10^{-4}	0.504826	0.50485	0.50487263	0.50487264
10^{-5}	0.389696	0.38962	0.38970223	0.38970229

z_{as} is the asymptotic estimate from (7), z_{GK} is the numerical result from [9], z is the present direct numerical computation, and z_{ex} is the numerical solution from exact formula (3).

size is used in the right half of the domain where the transition layer moves through. This mesh will be used throughout this paper, and better resolution is obtained by p-refinement, i.e. by increasing the basis polynomial order within each element. From Figure 1, we can see clearly that with perturbation δ as small as 0.01, the location of the transition layer, defined as the zero of the solution $u(z) = 0$, is of order one. Specifically, we obtain $z = 0.73746$ in this case.

Computations are conducted for different magnitudes of perturbation δ, and with different viscosity ν. To ensure steady states are reached, we require $\mathrm{d}u/\mathrm{d}t \simeq (u^{n+1} - u^n)/\Delta t < 10^{-12}$. Systematic p-refinement was conducted by increasing the order N of the basis polynomials in each element until resolution-independent solutions in space are obtained. In these computations we require the location of the transition layer to converge to eight significant digits, which in most cases require 20th-order ($N = 20$) spectral elements. In Tables I and II, we present locations of transition layer from our direct numerical computations and those from solution of the exact formulas (3), along with the asymptotic estimates from (7) and results from [9] for comparison. It can be seen that the direct numerical solutions are accurate for up to seven digits when compared with the exact solution. Also, the numerical results from [9] and those of asymptotic estimates agree well with the exact solutions in general. Details of the resolution independence tests are reported in Appendix A to verify the convergence of the simulations.

3. STOCHASTIC SUPERSENSITIVITY: FORMULATIONS

In this section, we consider the supersensitivity problem (1) when the perturbation δ is random. We present briefly the formulation of the generalized polynomial chaos expansion, as well as the formulation by perturbation method. We also consider brute-force Monte Carlo simulation for validation purposes.

3.1. Generalized polynomial chaos

The generalized polynomial chaos expansion is a representation of stochastic processes by polynomial functionals of random variables, i.e.

$$u(x,t;\omega) = \sum_{i=0}^{\infty} u_i(x,t)\Phi_i(\boldsymbol{\xi}(\omega)) \tag{9}$$

where $\boldsymbol{\xi}$ are multi-dimensional random variables as functions of the random parameter ω. Here the solution $u(x,t;\omega)$ becomes stochastic due to the random inputs. In principle, the expansion resides in an infinite dimensional random space of $\boldsymbol{\xi}$. In practice, one has to work in a finite-dimensional space and this is determined by the random inputs. Since the only random input in (1) is δ through the boundary condition, expansion (9) is one-dimensional. Therefore, the finite-term expansion takes the following form:

$$u(x,t;\omega) = \sum_{i=0}^{M} u_i(x,t)\Phi_i(\xi(\omega)) \tag{10}$$

where M is the highest order of the expansion. Depending on the distribution of the random variable ξ, different types of orthogonal polynomial bases are chosen. The appropriate correspondence is shown in Table III.

In this paper, we assume δ has a continuous distribution with bounded support. Thus, the Jacobi-chaos, i.e. an expansion in terms of beta random variables is employed. This includes the special case of Legendre-chaos which is in terms of uniform random variables. For detailed account of generalized polynomial chaos and their applications in multidimensional random spaces, see References [14, 26, 41].

Upon substituting (10) into (1), we obtain,

$$\sum_{i=0}^{M} \frac{\partial u_i(x,t)}{\partial t}\Phi_i + \sum_{i=0}^{M}\sum_{j=0}^{M} u_i(x,t)\frac{\partial u_j(x,t)}{\partial x}\Phi_i\Phi_j = \nu\sum_{i=0}^{M}\frac{\partial^2 u_i(x,t)}{\partial x^2}\Phi_i \tag{11}$$

where the explicit dependence of Φ on $\xi(\omega)$ is suppressed. Next a Galerkin projection is conducted to project the above equation onto the bases spanned by $\{\Phi_k\}_{k=0}^{M}$. By using the orthogonality of the bases

$$\langle\Phi_i\Phi_j\rangle = \langle\Phi_i^2\rangle\delta_{ij} \tag{12}$$

where δ_{ij} is the Kronecker delta and $\langle\cdot,\cdot\rangle$ denotes the ensemble average which is the inner product in the Hilbert space of the variable ξ, we obtain

$$\frac{\partial u_k}{\partial t} + \frac{1}{\langle\Phi_k^2\rangle}\sum_{i=0}^{M}\sum_{j=0}^{M} u_i\frac{\partial u_j}{\partial x}e_{ijk} = \nu\frac{\partial^2 u_k}{\partial x^2}, \quad \forall k \in [0, M] \tag{13}$$

Table III. Correspondence of the type of generalized polynomial chaos and their underlying random variables ($N \geqslant 0$ is a finite integer).

	Random variables $\boldsymbol{\xi}$	Polynomial bases $\{\Phi(\boldsymbol{\xi})\}$	Support
Continuous	Gaussian	Hermite-chaos	$(-\infty, \infty)$
	Gamma	Laguerre-chaos	$[0, \infty)$
	Beta	Jacobi-chaos	$[a, b]$
	Uniform	Legendre-chaos	$[a, b]$
Discrete	Poisson	Charlier-chaos	$\{0, 1, 2, \ldots\}$
	Binomial	Krawtchouk-chaos	$\{0, 1, \ldots, N\}$
	Negative binomial	Meixner-chaos	$\{0, 1, 2, \ldots\}$
	Hypergeometric	Hahn-chaos	$\{0, 1, \ldots, N\}$

where $e_{ijk} = \langle \Phi_i \Phi_j \Phi_k \rangle$. Together with $\langle \Phi_k^2 \rangle$, these coefficients can be evaluated from the definition of the generalized polynomial chaos analytically. Equation (13) is a set of $(M+1)$ coupled non-linear equations. Here we employ again the semi-implicit scheme where the viscous terms are treated implicitly and the non-linear terms explicitly.

The boundary conditions are also expanded in the form of (10). For example, if we assume $\delta \in (0, \varepsilon)$ is a beta random variable $Be^{(\alpha,\beta)}(0, \varepsilon)$ with $\alpha, \beta > -1$, the left boundary condition can be rewritten as

$$u(-1) = 1 + \delta = (1 + \bar{\delta}) + \sigma\xi \tag{14}$$

where $\bar{\delta}$ is the mean of δ and $\xi \in (-1, 1)$ is a beta random variable $Be^{(\alpha,\beta)}(-1, 1)$ with zero mean and probability density function

$$f(\xi) = \frac{\Gamma(\alpha + \beta + 2)}{2^{\alpha+\beta+1}\Gamma(\alpha + 1)\Gamma(\beta + 1)}(1 - \xi)^{\alpha}(1 + \xi)^{\beta} \tag{15}$$

Here σ scales as its standard deviation. Under this expression, the generalized polynomial chaos expansion for the left boundary condition takes the form,

$$u_0(-1) = 1 + \bar{\delta}, \quad u_1(-1) = \sigma, \quad u_k(-1) = 0 \text{ for } k \geqslant 2 \tag{16}$$

The right boundary condition $u(1) = -1$ takes a simpler expansion form of $u_0(1) = -1$ and $u_k(1) = 0$ for $k \geqslant 1$.

3.2. Perturbation method

Again $\delta \in (0, \varepsilon)$ is a random variable and we further assume $\varepsilon \ll 1$. The left boundary condition is written as

$$u(-1) = 1 + \delta = \mu + \xi \tag{17}$$

where $\mu = 1 + \bar{\delta}$ is the mean value and $\xi \in (-\varepsilon/2, \varepsilon/2)$. In the perturbative approach, the stochastic quantities are expanded via a Taylor series around the mean value of the random inputs, i.e.

$$u(x, t; \omega) = u_0(x, t) + \xi u_1(x, t) + \xi^2 u_2(x, t) + \cdots \tag{18}$$

where

$$u_k(x,t) = k! \left.\frac{\partial^k u(x,t;\omega)}{\partial^k \xi}\right|_{\xi(\omega)=\mu}, \quad k = 0, 1, 2, \ldots \tag{19}$$

Upon substituting expansion (18) into (1) and equating the terms of different orders, under the assumption that $O(1) \gg O(\xi) \gg O(\xi^2) \gg \cdots$, we obtain the following set of equations:

$$O(\xi^0): \ \frac{\partial u_0}{\partial t} + u_0 \frac{\partial u_0}{\partial x} = \nu \frac{\partial^2 u_0}{\partial x^2} \tag{20}$$

$$O(\xi^k): \ L(u_k) = F_k(u_0, \ldots, u_{k-1}), \quad k \geqslant 1 \tag{21}$$

where

$$L(u_k) = \frac{\partial u_k}{\partial t} + \frac{\partial (u_0 u_k)}{\partial x} - \frac{\partial^2 u_k}{\partial x^2} \tag{22}$$

is a linear operator, and the right-hand side terms are

$$F_1 = 0, \quad F_2 = -u_1 \frac{\partial u_1}{\partial x}, \quad F_3 = -\frac{\partial (u_1 u_2)}{\partial x}, \quad F_4 = -\frac{\partial (u_1 u_3)}{\partial x} - u_2 \frac{\partial u_2}{\partial x}, \ldots \tag{23}$$

The boundary conditions are matched by the orders of ξ as well. For the left boundary, $u_0(-1) = \mu, u_1(-1) = 1$ and $u_k(-1) = 0$ for $k \geqslant 2$; for the right boundary, $u_0(1) = -1$ and $u_k(1) = 0$ for $k \geqslant 1$.

3.3. Monte Carlo simulation

The brute-force Monte Carlo simulation (MC) is also employed, where samples of $\delta \in (0, \varepsilon)$ are drawn according to its distribution and the deterministic solver is executed for each sample input. Two deterministic solvers are available: the iterative solver of the exact solution (2) and (3); and the direct numerical integration of (1). Due to the supersensitive nature of the problem, it is non-trivial to construct robust initial conditions for the iterative solver to converge for all the random realizations. Thus, we employ the direct integration of Burgers' equation. (Note that this is the traditional approach in Monte Carlo simulations as the exact solutions are not known in general.) This approach, however, is time consuming, especially for the supersensitivity problem which reaches steady states on a very slow time scale t^* (see Equation (6)). Here we conduct MC simulations for one specific case of ν and δ to validate the results obtained by generalized polynomial chaos.

4. STOCHASTIC SUPERSENSITIVITY: NUMERICAL RESULTS

In this section, we present the numerical results of the viscous Burgers' equation subject to random perturbations on the boundary condition (1). We focus on the statistics of the location of the transition layer at steady state. In particular, we document the mean position of the transition layer and its standard deviation, denoted as $\bar{z}$ and σ_z hereafter, respectively. The same mesh as shown in Figure 1 is used.

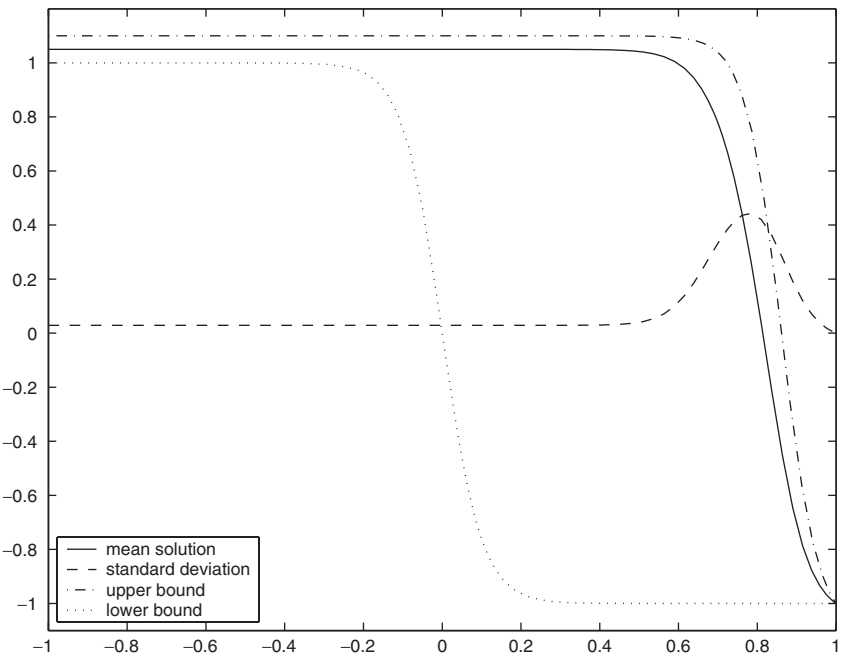

Figure 2. Stochastic solutions by Legendre-chaos with $\delta \sim U(0, 0.1)$ and $v = 0.05$. The upper and lower bounds are the deterministic solutions corresponding to the bounds of the random inputs, $\delta = 0.1$ and 0, respectively.

4.1. Uniform random input

We assume $\delta \sim U(0, \varepsilon)$ is a uniform random variable in $(0, \varepsilon)$, which is a special case of beta random variable with $\alpha = \beta = 0$, i.e. $\delta \sim Be^{(0,0)}(0, \varepsilon)$.

4.1.1. Legendre-chaos expansion. In Figures 2 and 3, the stochastic solutions by Legendre-chaos with $\delta \sim U(0, 0.1)$ are shown at two viscosity values $v = 0.05$ and 0.1, respectively. The mean solution profile, the standard deviation, and the upper and lower bounds of the solution are plotted. The upper and lower bounds are the deterministic solutions with boundary condition corresponding to the bounds of the random inputs, i.e. $\delta = 0.1$ and 0 in this case. They give the extreme solutions which constitute a rather wide response interval, and the mean location of the transition layer is not centred in the interval. The standard deviation peaks near the mean location of the transition layer. A 10% random input results in more than 40% peak response of the random output for $v = 0.05$. Also, the profiles of the standard deviation give us sharper estimations of the variation of the stochastic output.

The stochastic solutions in Figures 2 and 3 are obtained by high-order discretization, with 10th-order chaos expansion ($M = 10$) and 22th-order ($N = 22$) spectral elements. In Table IV, we tabulate the results at $v = 0.05$ and 0.1 under uniform random input $\delta \sim U(0, \varepsilon)$, with different values of ε. Examples of the detailed resolution refinement tests are shown in

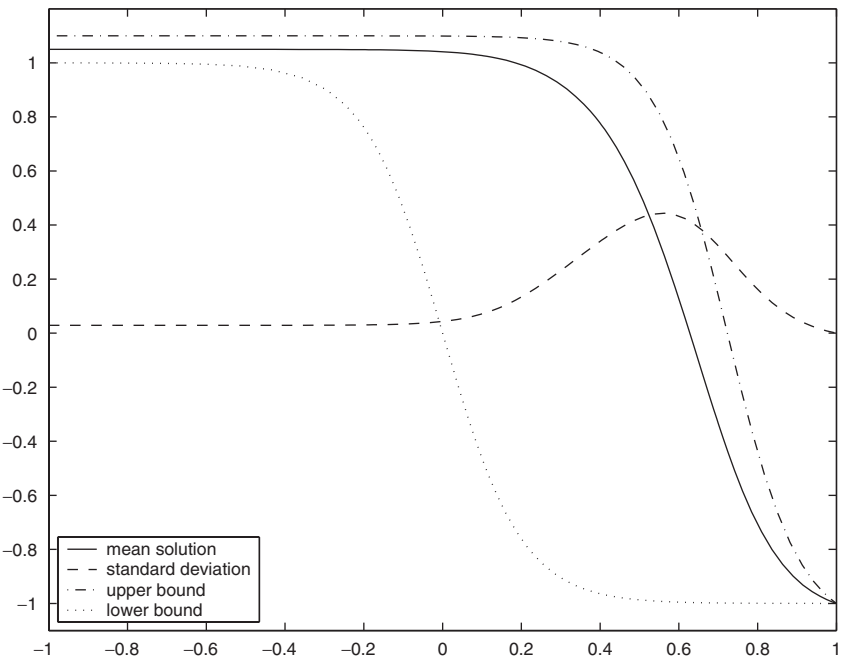

Figure 3. Stochastic solutions by Legendre-chaos with $\delta \sim U(0, 0.1)$ and $\nu = 0.1$. The upper and lower bounds are the deterministic solutions corresponding to the bounds of the random inputs, $\delta = 0.1$ and 0, respectively.

Table IV. The mean locations ($\bar{z}$) of the transition layer and their corresponding standard deviations (σ_z) subject to uniform random perturbation $\delta \sim U(0, \varepsilon)$ on the boundary condition.

	$\nu = 0.05$			$\nu = 0.1$		
ε	10^{-1}	10^{-2}	10^{-3}	10^{-1}	10^{-2}	10^{-3}
$\bar{z}$	0.81390488	0.69062979	0.57410655	0.62781226	0.38156021	0.15912335
σ_z	0.41403291	0.37864690	0.37322135	0.41400822	0.37591977	0.30390529

Appendix B. Note that in these cases, even very small random perturbation of 0.1% can result in more than 30% stochastic response in the output.

One of the advantages of the generalized polynomial chaos expansions is that the solutions take an analytical form in terms of the random inputs. Thus, one can in principle apply various manipulations to obtain the desired output statistics. Here we show the probability density functions of the solutions at various spatial locations, in particular, at $x = 0.6, 0.7, 0.8$ and 0.9 which are located inside the transition layer. The results with $\delta \in U(0, 0.1)$ are shown in Figures 4 and 5. Figure 4 shows the results at $\nu = 0.05$. In this case the point $x = 0.6$ is located at the entrance of the transition layer, and the PDF here has a clear cutoff on the right and a tail on the left. The stochastic Gibb's phenomenon is present as we observe numerical oscillations. Inside the transition layer at $x = 0.7$ and 0.8, the PDFs are wider, with cutoff on

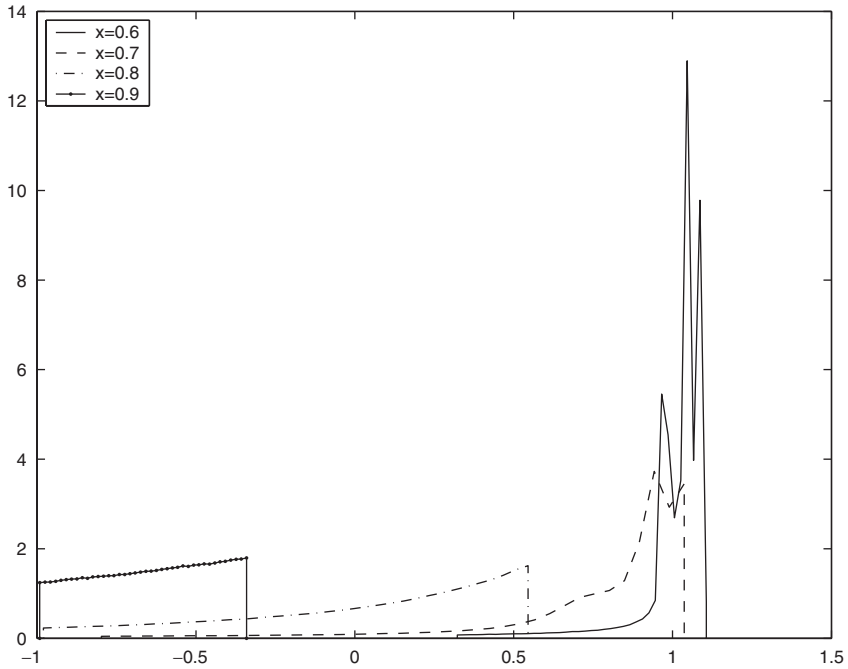

Figure 4. Probability density functions at various locations for $\delta \sim U(0, 0.1)$ and $v = 0.05$. Gibb's oscillations are present at $x = 0.6$ and 0.5.

the left as well. Near the end of the transition layer at $x = 0.9$, the PDF becomes narrower. Not all the PDFs are uniform. Figure 5 shows the results for $v = 0.1$. Here the first point $x = 0.6$ is already inside the transition layer. Again the PDF is sharp near the end of the layer at $x = 0.9$. From these results, we observe that the uniform random input at the left boundary is widened inside the transition layer, and sharpened near the end of the layer.

4.1.2. Monte–Carlo simulations. Monte Carlo simulations based on the direct numerical simulations of (1) are conducted for the case of $v = 0.05, \delta \sim U(0, 0.1)$ to validate the results obtained by generalized polynomial chaos. Because of the slow convergence $O(\sqrt{n})$ where n is the number of realizations, we relax the spatial resolutions as the sampling error will be predominant. In particular, we require $\mathrm{d}u/\mathrm{d}t < 10^{-7}$ for steadiness and employ $N = 14$ spectral element. Deterministic results in Appendix A show that at this spatial resolution the location of transition layer can be accurate up to five significant digits, which ensures the spatial errors to be subdominant. The results of Monte Carlo simulations are shown in Table V. It is seen that as the number of realization increases, the Monte Carlo solutions converge, non-monotonically, to the solution of Legendre-chaos in Table IV. With $n = 10\,000$, the mean and standard deviation agree with the Legendre-chaos results in three significant digits, and the difference is certainly within the sampling error range of the MC simulations. Furthermore, in Figures 6 and 7 we show the solution PDFs by Monte Carlo computation with $n = 10\,000$

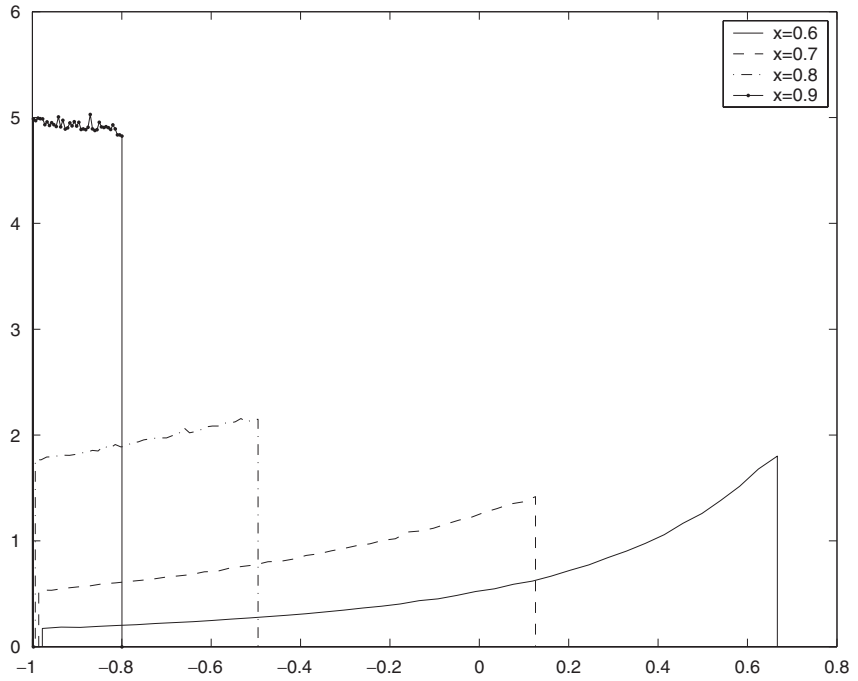

Figure 5. Probability density functions at various locations for $\delta \sim U(0, 0.1)$ and $v = 0.1$.

Table V. The mean location of the transition layer ($\bar{z}$) and its standard deviation (σ_z) from Monte Carlo simulations.

	$n = 100$	$n = 1000$	$n = 2000$	$n = 5000$	$n = 10000$	Legendre-chaos
$\bar{z}$	0.81853	0.81407	0.81448	0.81436	0.81397	0.81390488
σ_z	0.38705	0.41801	0.41699	0.41676	0.41418	0.41403291

n is the number of realizations, $\delta \sim U(0, 0.1)$ and $v = 0.05$. Also shown are the converged Legendre-chaos solutions for comparison.

realization at the four points $x = 0.6, 0.7, 0.8,$ and 0.9, along with the PDFs from Legendre-chaos expansion. We observe good agreements between the two sets of results, in spite of the Gibb's oscillations of Legendre-chaos near the sharp corner. These results serve as validations of the Legendre-chaos computations.

4.1.3. Perturbation methods. We also solve the case of $v = 0.05$ and $\delta \sim U(0, 0.1)$ by a perturbation method. The results are tabulated in Table VI. The spectral element order is $N = 20$ which ensures convergence in physical space. Up to a fourth-order perturbative expansion is employed. It is seen that while the mean location is close to the converged solution of polynomial chaos computation, the standard deviations have as high as 20% error compared to the chaos solution. Also, there is no clear sign of convergence as we increase the order of

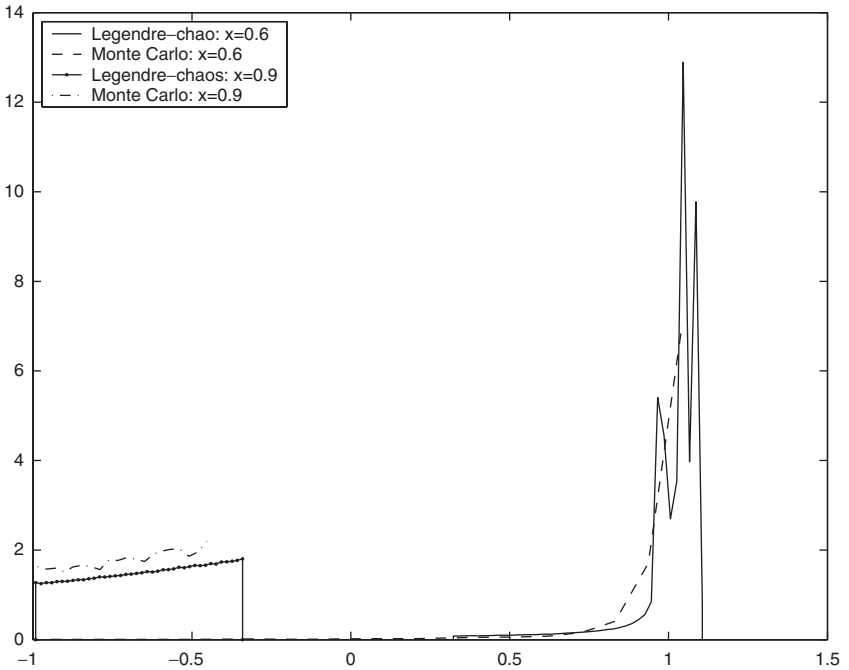

Figure 6. Probability density functions at $x = 0.6$ and 0.9 for $\delta \sim U(0, 0.1)$ and $v = 0.05$ by Monte Carlo simulation and Legendre-chaos expansion. (The oscillations at $x = 0.9$ are due to Gibb's phenomenon.).

expansion. In fact, the first-order results are better than the rest, and the standard deviations of the third-, fourth-order results are noticeably worse than the first- and second-order results.

Two reasons can be attributed to the poor resolution of the perturbation method. First, although the random input is only 10% in maximum value, the response of the solution has fluctuations as high as 40%, as shown by the generalized polynomial chaos computation. This is clearly out of the effective regime of perturbation methods, and explains the relatively poor results, especially in standard deviation. Second, the nature of perturbative approach does not guarantee convergence as one increases the order of expansion. In fact, for a given magnitude of perturbation, there exists an optimal expansion order that gives the best result, see for example References [52–55]. This is a well-known fact in asymptotic analysis, and it appears that the first-order expansion is optimal in this case.

4.2. 'Truncated' Gaussian random input $G(a, b)$

In this section, we model the random input at boundary with a 'Gaussian-like' distribution. Gaussian is the most commonly used model when the nature of the actual random inputs is unclear. Here, to ensure the perturbation is small and bounded, we 'truncate' the support of the Gaussian distribution. Instead of simply truncating the tails and renormalizing the PDF to ensure the total CDF is unity, we employ a 'truncated Gaussian' model developed in Reference [43]. This model uses a Jacobi-chaos expansion to represent the Gaussian PDF, and is denoted

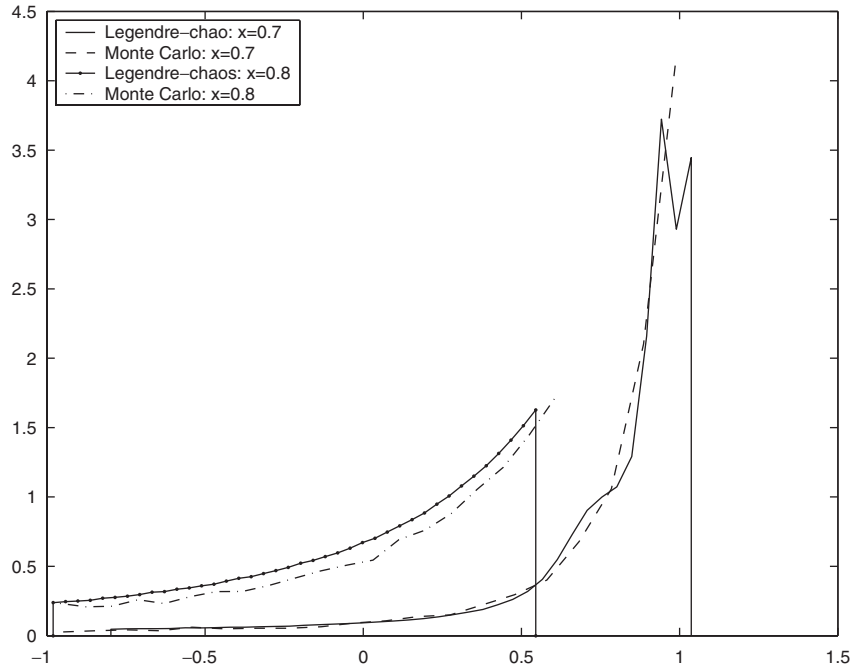

Figure 7. Probability density functions at $x = 0.7$ and 0.8 for $\delta \sim U(0, 0.1)$ and $v = 0.05$ by Monte Carlo simulation and Legendre-chaos expansion.

Table VI. The mean location of the transition layer ($\bar{z}$) and its standard deviation (σ_z) from the perturbation method.

	$k = 1$	$k = 2$	$k = 3$	$k = 4$	Legendre-chaos
$\bar{z}$	0.82316323	0.82381706	0.82381706	0.82379866	0.81390488
σ_z	0.34931667	0.34896352	0.32800483	0.32801031	0.41403291

k is the order of the perturbative expansion, $\delta \sim U(0, 0.1)$ and $v = 0.05$. Also shown are the converged results from Legendre-chaos.

as $G(a, b)$ where (a, b) is the bounded support of the distribution. In Reference [43] it is used to circumvent the ill-posedness of the semi-discrete system for diffusion equation resulted from the tails of Gaussian distribution. Here we employ the fifth-order Jacobi-chaos model with $\alpha = \beta = 10$, as shown in Figure C1. It can be seen that this model approximates Gaussian distribution very closely, and has bounded support, i.e. no tails. Details of the truncated Gaussian modeling can be found in Reference [43]. A brief review is included in Appendix C.

In Table VII, we show the mean location of the transition layer and its standard deviation with $\delta \sim G(0, 0.1)$ as the random perturbation on the left boundary condition of (1). These solutions are obtained by 9th-order Jacobi-chaos with $\alpha = \beta = 10$ ($M = 9$) and 22th-order spectral elements ($N = 22$) to ensure the solutions converge to eight significant digits. Compared to the uniform perturbation $\delta \sim U(0, 0.1)$, under 'Gaussian' perturbation $\delta \sim G(0, 0.1)$

Table VII. The mean location of the transition layer ($\bar{z}$) and its standard deviation (σ_z) with truncated Gaussian random inputs $\delta \sim G(0, 0.1)$, for $v = 0.05$ and 0.1.

	$v = 0.05, \delta \sim G(0, 0.1)$	$v = 0.1, \delta \sim G(0, 0.1)$
$\bar{z}$	0.82217889	0.64435795
σ_z	0.13195896	0.13367561

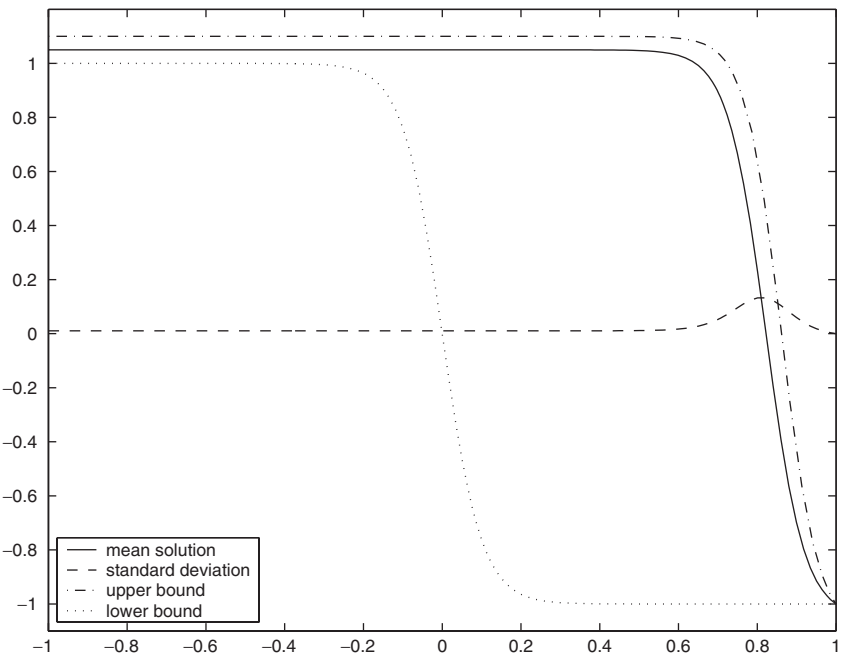

Figure 8. Stochastic solution by Jacobi-chaos ($\alpha = \beta = 10$) with $\delta \sim G(0, 0.1)$ and $v = 0.05$. The upper and lower bounds are the deterministic solutions corresponding to the bounds of the random inputs $\delta = 0.1$ and 0, respectively.

the mean location of transition layer is further to the right, but with much smaller standard deviation.

The solutions with $\delta \sim G(0, 0.1)$ are shown in Figures 8 and 9, for $v = 0.05$ and 0.1, respectively. The corresponding PDF of the solutions at locations $x = 0.6, 0.7, 0.8$ and $x = 0.9$ are shown in Figures 10 and 11. Again, point $x = 0.6$ is located at the beginning of the transition layer for $v = 0.05$. We observe from Figure 10 that the distribution is widened inside the transition layer at $x = 0.7$ and 0.8, and is sharpened near the end of the layer at $x = 0.9$. This sharpening process is clearly seen from Figure 11, which is for the case of $v = 0.1$. In this case, the first point $x = 0.6$ is inside the transition layer. Since the random inputs at the boundary are extremely close to Gaussian, we naturally compare the PDFs at these locations to Gaussian distributions. In Figures 12 and 13, the PDFs at these locations for $v = 0.05$

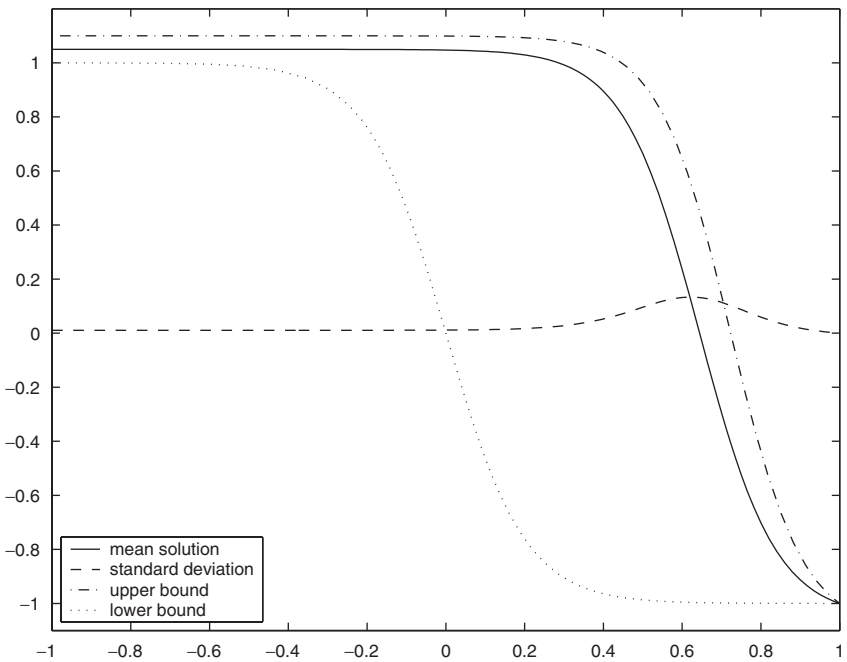

Figure 9. Stochastic solution by Jacobi-chaos ($\alpha = \beta = 10$) with $\delta \sim G(0, 0.1)$ and $v = 0.1$. The upper and lower bounds are the deterministic solutions corresponding to the bounds of the random inputs $\delta = 0.1$ and 0, respectively.

are shown. Also shown with dashed lines are the reference Gaussian PDFs obtained at these locations with same mean values and standard deviations. It is seen that except at $x = 0.9$, the distributions are non-Gaussian. The PDFs are skewed and with clear cutoff at the tails. Near the end of the transition layer at $x = 0.9$, the skewness is smoothed and the distribution becomes close to Gaussian (see Figure 13). Note that although the PDF is close to Gaussian, it is *not* Gaussian as it does not possess long tails. In Figures 14 and 15, the comparisons of the PDFs at these locations are shown for $v = 0.1$, and we observe similar results.

5. SUMMARY AND CONCLUSIONS

In this paper the supersensitivity of the viscous Burgers' equation subject to small perturbations on the boundary condition was studied numerically. We presented detailed simulations for both the *deterministic* and *stochastic* supersensitivity problems. High-resolution stochastic simulations are conducted by high-order spectral/hp element method in physical space, and high-order generalized polynomial chaos expansions in random space. Extensive numerical experiments are conducted to ensure the results are accurate and convergent.

It is found that small random perturbations on the upstream boundary condition can result in *order one* changes on the eventual mean location of the transition layer. The uncertainty of this transition layer, measured by the standard deviation of its mean location, is also high. As high as

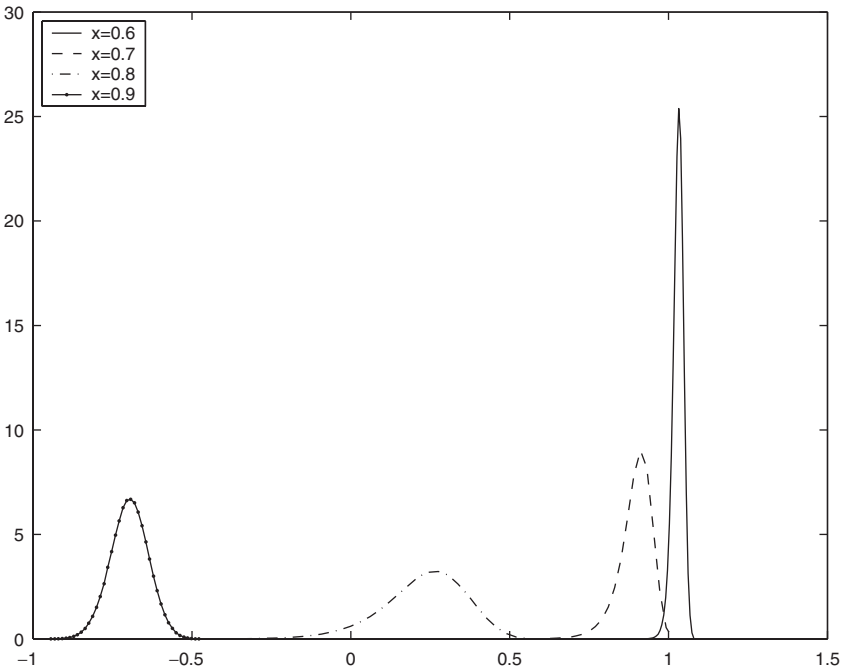

Figure 10. Probability density functions at various locations ($\delta \sim G(0, 0.1)$ and $v = 0.05$).

30% output uncertainty can be obtained by only 0.1% random input. The generalized polynomial chaos expansion is shown to be capable of capturing this highly non-linear problem accurately. Its convergence is demonstrated by resolution refinements both in physical space and random space. Its accuracy is verified by conducting Monte Carlo simulations. Perturbation methods of up to fourth-order expansions are also employed. The resolution, however, is poor, due to its inherent limitations. High-order perturbation methods do not offer advantages compared to first-order method, at least for this particular problem.

The problem considered here is inherently one-dimensional in random space, i.e. the boundary perturbation is described by a random variable. For general problems with *random processes* as input, multi-dimensional generalized polynomial chaos is required. Such problems are treated in References [14, 41, 56]; for multi-dimensional Wiener–Hermite expansions, see Reference [32] and the references therein. The 'truncated' Gaussian model based on Jacobi-chaos expansion is proposed in this paper to circumvent the difficulties caused by the Gaussian tails; however, its multi-dimensional expansion property remains an open issue.

We also remark that special care is needed if one is to apply generalized polynomial chaos to martingales, as Brownian motion and Poisson process are the only normal martingales with the classical chaos representation property (CRP) (see Reference [40, pp. 88]). However, most stochastic processes encountered in engineering problems are not martingales, and convergence of polynomial type representations of stochastic problems, which includes generalized polynomial chaos, has been proved by Babuška *et al*. [45].

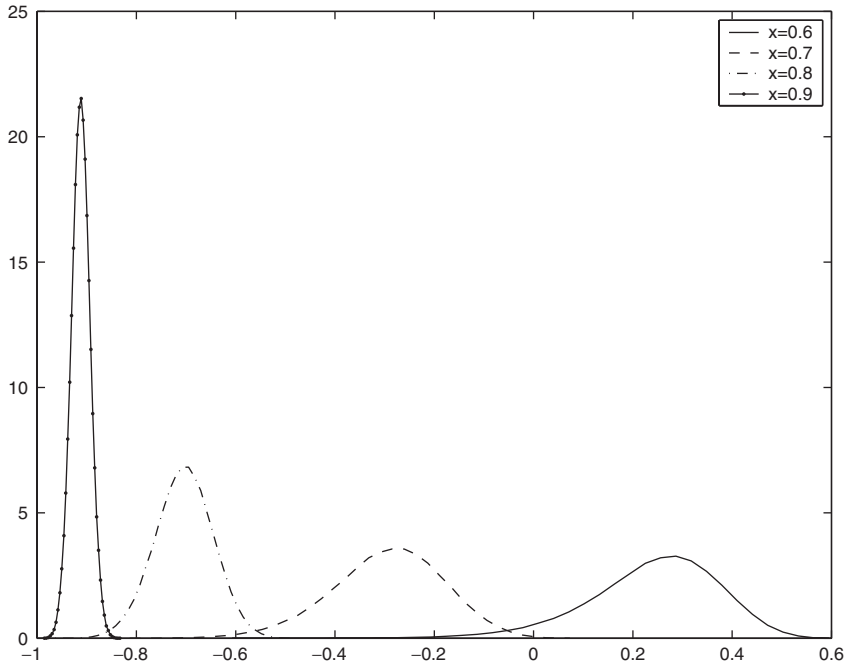

Figure 11. Probability density functions at various locations ($\delta \sim G(0, 0.1)$ and $v = 0.1$).

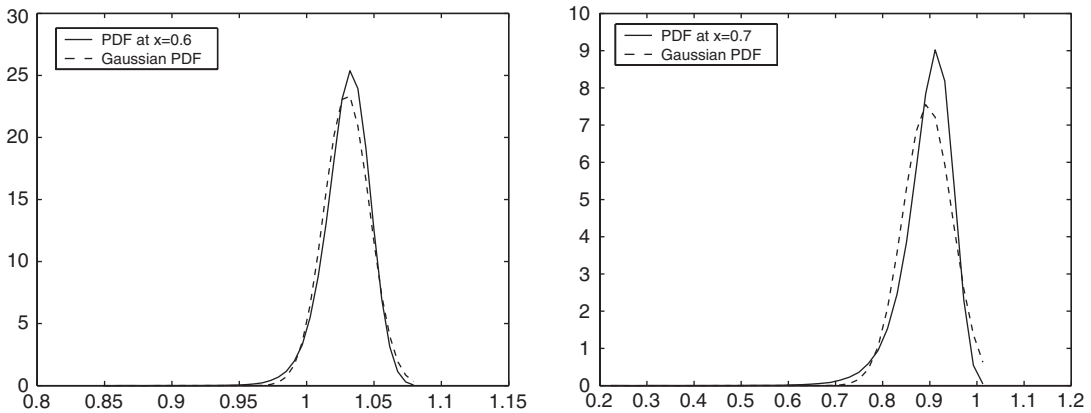

Figure 12. Probability density functions with $v = 0.05$, $\delta \sim G(0, 0.1)$. Left: $x = 0.6$; Right: $x = 0.7$.

The stochastic supersensitivity problem is a natural extension of its well-studied deterministic counterpart. It is a highly non-linear problem where small random inputs can result in large stochastic outputs, and ignoring the uncertain inputs will completely 'miss the picture'. We expect that similar problems will arise in compressible fluid mechanics problems, where stronger non-linearities are present.

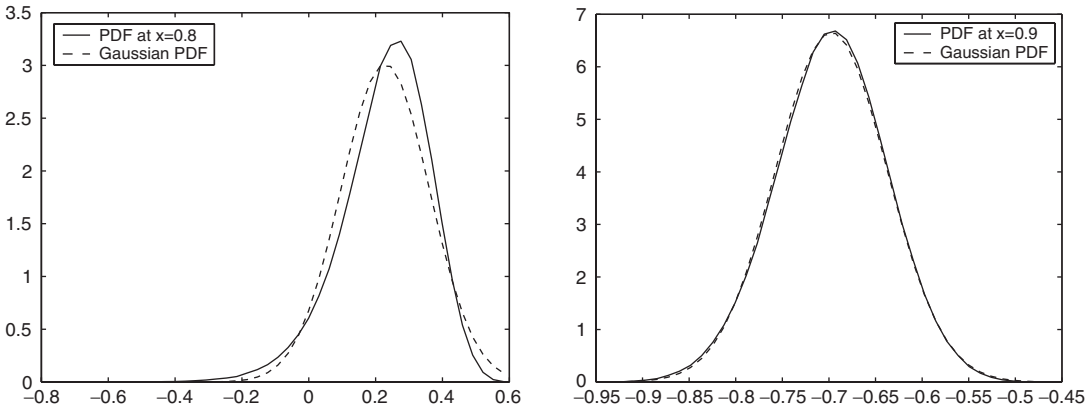

Figure 13. Probability density functions with $v = 0.05$, $\delta \sim G(0, 0.1)$. Left: $x = 0.8$; Right: $x = 0.9$.

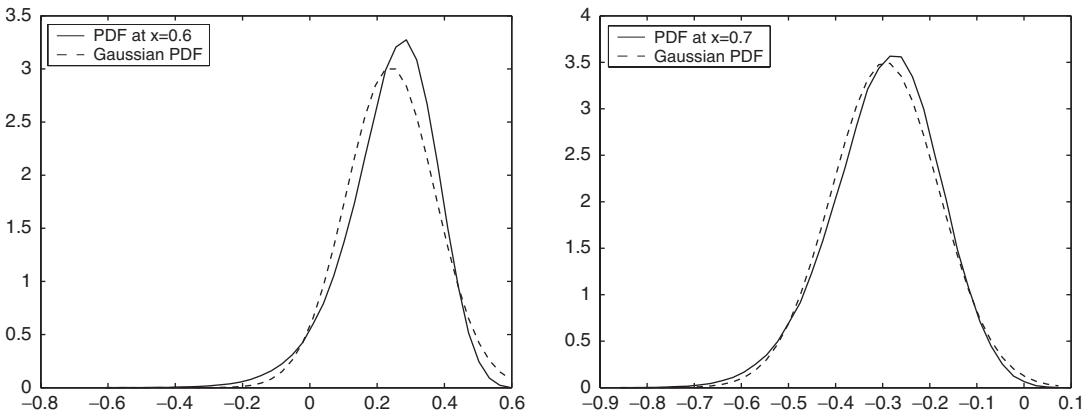

Figure 14. Probability density functions with $v = 0.1$, $\delta \sim G(0, 0.1)$. Left: $x = 0.6$; Right: $x = 0.7$.

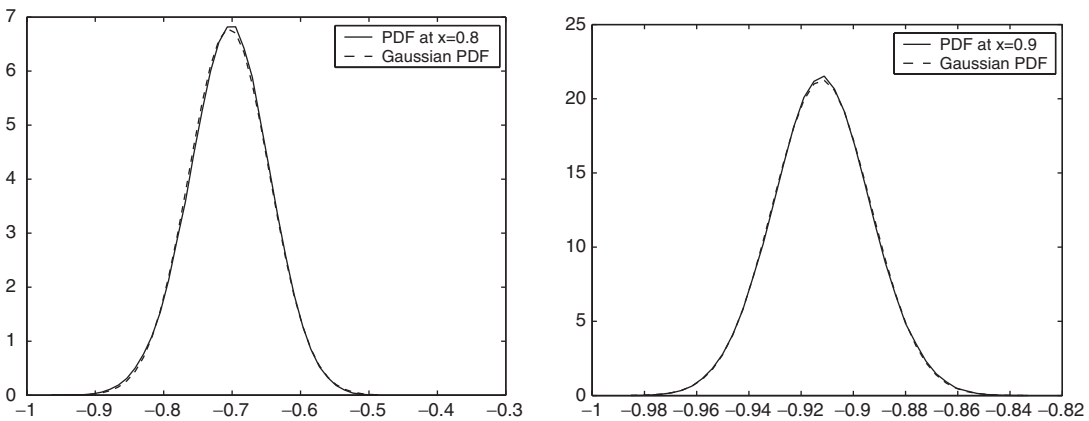

Figure 15. Probability density functions with $v = 0.1$, $\delta \sim G(0, 0.1)$. Left: $x = 0.8$; Right: $x = 0.9$.

APPENDIX A: NUMERICAL RESULTS FOR DETERMINISTIC SUPERSENSITIVITY

Here we summarize the deterministic results of the direct numerical simulations of problem (1). In Tables AI and AII we tabulate the solutions at $\nu = 0.05$ and 0.1, respectively. Different values of δ are considered, and the orders of spectral elements are increased in order to obtain resolution independent solutions. It can be seen that with 20th-order spectral elements ($N = 20$), the locations of transition layer converge with eight significant digits, and they agree with exact solutions to seven digits.

Table AI. The locations of the transition layer at $\nu = 0.05$ with different values of perturbation δ.

	$\delta = 10^{-1}$	$\delta = 10^{-2}$	$\delta = 10^{-3}$	$\delta = 10^{-4}$	$\delta = 10^{-5}$
$T_{\max}$	60	400	3480	13 500	88 000
$N = 10$	0.86162068	0.73745817	0.62032373	0.50485891	0.38969812
$N = 12$	0.86161448	0.73746021	0.62031203	0.50487016	0.39970204
$N = 14$	0.86161302	0.73746023	0.62030992	0.50487220	0.38970225
$N = 16$	0.86161270	0.73746017	0.62030961	0.50487256	0.38970223
$N = 18$	0.86161263	0.73746015	0.62030958	0.50487262	—
$N = 20$	0.86161262	—	0.62030957	0.50487263	—
$N = 21$	—	—	—	—	—
Exact	0.86161262	0.73746015	0.62030957	0.50487264	0.38970229

N is the order of spectral elements, and the dash '—' indicates that the number there is the same as the one above it. The results from exact formula are also shown.

Table AII. The locations of the transition layer at $\nu = 0.1$ with different values of perturbation δ.

	$\delta = 10^{-1}$	$\delta = 10^{-2}$	$\delta = 10^{-3}$	$\delta = 10^{-4}$	$\delta = 10^{-5}$
$N = 10$	0.72322540	0.47992739	0.24142359	0.052673383	0.0055171392
$N = 12$	0.72322524	0.47492741	0.24142361	0.052669622	0.0055085668
$N = 14$	0.72322525	0.47492741	—	0.052669616	0.0055085545
$N = 16$	—	—	—	—	—
Exact	0.72322525	0.47492741	0.24142361	0.052669612	0.0055085559

N is the order of spectral elements, and the dash '—' indicates that the number there is the same as the one above it. The results from exact formula are also shown.

APPENDIX B: NUMERICAL RESULTS FOR STOCHASTIC SUPERSENSITIVITY

In Table BI, the numerical results of Burgers' equation (1) are shown for $\nu = 0.05$ and $\delta \sim U(0, 0.1)$. The mean locations of the transition layer and their standard deviations are tabulated, with different Legendre-chaos orders M and spectral element orders N. It can be seen that as the expansion orders, both N in physical space and M in random space, increase, the results converge to resolution-independent values. In this case, they are $\bar{z} = 0.81390488$ and $\sigma_z = 0.41403291$, which are the same as the reference values obtained with a higher resolution of $M = 10$ and $N = 22$.

Table BI. The stochastic solution of the locations of the transition layer at $v = 0.05$ listed in form of $(\bar{z}, \sigma_z)$, where $\bar{z}$ is the mean location and σ_z its standard deviation.

	$N = 14$	$N = 18$	$N = 20$
$M = 1$	0.81459325, 0.37660585	0.81459294, 0.37660750	0.81459294, 0.37660751
$M = 2$	0.81394065, 0.41100263	0.81394090, 0.41099364	0.81394090, 0.41099350
$M = 3$	0.81390669, 0.41382150	0.81390671, 0.41382035	0.81390671, 0.41382035
$M = 4$	0.81390493, 0.41401936	0.81390498, 0.41401904	0.81390498, 0.41401897
$M = 5$	0.81390481, 0.41403293	0.81390489, 0.41403210	0.81390489, 0.41403202
$M = 6$	—, 0.41403393	0.81390488, 0.41403291	0.81390488, 0.41403286
$M = 7$	—, —	—, 0.41403296	—, 0.41403291
$M = 8$	—, —	—, —	—, —

M is the order of Legendre-chaos; N is the order of spectral elements. The dash '—' indicates that the number there is the same as the one above it. The reference values obtained by $M = 10$ and $N = 22$ are (0.81390488, 0.41403291).

Similar resolution-independence tests were conducted for all the cases reported in this paper, and they are not further tabulated here.

APPENDIX C: THE TRUNCATED GAUSSIAN MODEL $G(a, b)$

The truncated Gaussian model was developed in Reference [43] in order to circumvent the mathematical difficulty resulted from the tails of Gaussian distribution. It is an approximation of Gaussian distributions by Jacobi-chaos expansion. The approximation can be improved either by increasing the order of expansion, or by adjusting the parameters in the Jacobi-chaos definition. The important property of the model is that it has bounded support, i.e. no tails. This can be used as an alternative in practical applications, where the random inputs resemble Gaussian distributions *and* the boundedness of the supports is critical to the solution procedure. Here we briefly review its construction from [43].

Suppose $y(\omega)$ is a random variable with continuous distribution function $G(y)$ and probability density function (PDF) $g(y)$ that satisfies $G(y) = \int_{-\infty}^{y} g(y)\,\mathrm{d}y$. Let $\{\Phi(\xi)\}$ be a set of generalized polynomial chaos whose underlying random variable ξ has distribution function $F(\xi)$ and PDF $f(\xi)$ such that $F(\xi) = \int_{-\infty}^{\xi} f(\xi)\,\mathrm{d}\xi$. The representation of y takes the form,

$$y(\omega) = \sum_{k=0}^{M} y_k \Phi_k(\xi), \quad y_k = \frac{\langle y, \Phi_k(\xi)\rangle}{\langle \Phi_k^2(\xi)\rangle} \tag{C1}$$

Evaluation of the inner product $\langle \cdot, \cdot \rangle$ in the numerator needs caution as in most cases y and ξ belong to two different probability spaces. This difficulty can be circumvented by mapping both y and ξ to the space defined by the uniform random variable, i.e.

$$y(\omega) = G^{-1}(u(\omega)), \quad \xi(\omega) = F^{-1}(u(\omega)) \tag{C2}$$

where $u(\omega) \in U(0, 1)$ is the uniform random variable in $(0, 1)$. Thus,

$$y_k = \frac{\langle y, \Phi_k(\xi)\rangle}{\langle \Phi_k^2(\xi)\rangle} = \frac{1}{\langle \Phi_k^2\rangle} \int_0^1 G^{-1}(u)\Phi_k(F^{-1}(u))\,\mathrm{d}u \tag{C3}$$

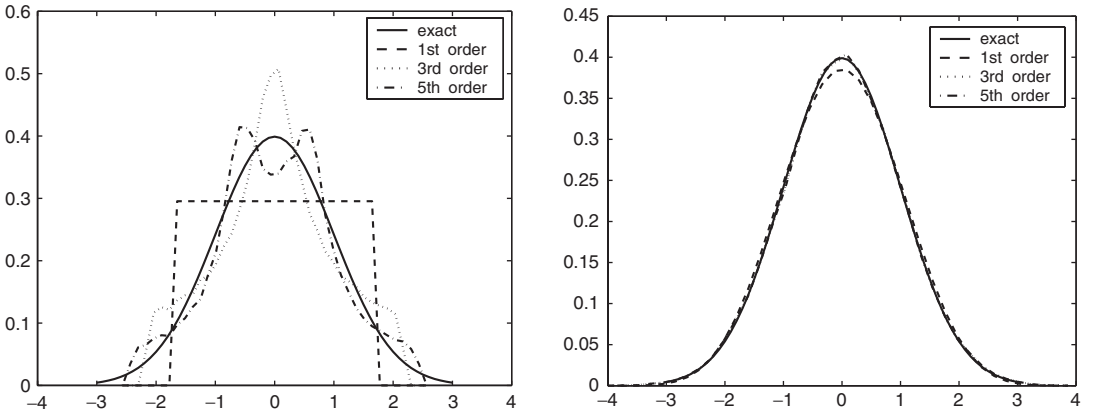

Figure CI. Approximated Gaussian random variables by Jacobi-chaos; Left: $\alpha = \beta = 0$, Right: $\alpha = \beta = 10$.

Table CI. Approximating Gaussian via Jacobi-chaos: expansion coefficients y_k and errors.

	$\alpha = \beta = 0$	$\alpha = \beta = 2$	$\alpha = \beta = 4$	$\alpha = \beta = 6$	$\alpha = \beta = 8$	$\alpha = \beta = 10$
y_1	1.69248	8.7827(−1)	6.6218(−1)	5.5273(−1)	4.8399(−1)	4.3575(−1)
ε_2	4.51704(−2)	8.25346(−3)	3.46301(−3)	2.00729(−3)	1.38842(−3)	1.07231(−3)
ε_4	1.35894	7.05024(−1)	4.79089(−1)	3.63557(−1)	2.93246(−1)	2.45916(−1)
y_3	4.8399(−1)	7.5493(−2)	2.6011(−2)	1.2216(−2)	6.77970(−3)	4.17792(−3)
ε_2	1.17071(−2)	8.51816(−4)	4.49245(−4)	4.23983(−4)	4.33894(−4)	4.45282(−4)
ε_4	5.02097(−1)	7.97474(−2)	3.33201(−2)	2.40064(−2)	2.21484(−2)	2.22539(−2)
y_5	2.7064(−1)	1.9959(−2)	2.9936(−3)	2.3531(−4)	−3.30888(−4)	−4.19539(−4)
ε_2	5.04838(−3)	3.97059(−4)	3.96880(−4)	4.22903(−4)	4.28283(−4)	4.25043(−4)
ε_4	2.55526(−1)	2.29373(−2)	1.92101(−2)	2.15095(−2)	2.06846(−2)	2.08317(−2)

(ε_2 is the error in variance; ε_4 is the error in kurtosis. There is no error in mean.) $y_k = 0$ when k is even.

This integral is defined the closed domain $[0, 1]$ and can be evaluated by Gaussian quadrature with accuracy. The analytical form of the inversion (C2) is not known in general, and numerical inversion is needed. Examples of this kind of representation can be found in Reference [26].

Now assume $y(\omega) \sim N(0, 1)$ is a standard Gaussian variable, and we use the Jacobi-chaos $\{\Phi(\xi)\}$ to represent it. Here $\xi \sim Be^{(\alpha,\beta)}(-1, 1)$ is a beta random variable defined in $(-1, 1)$ with parameters $\alpha, \beta > -1$ and probability density function (15). Due to the symmetry of Gaussian distribution, we set $\alpha = \beta$ in the Jacobi-chaos.

In Figure C1 the PDFs of the Jacobi-chaos approximations are plotted, for values of $\alpha = \beta =$ 0 and 10. For $\alpha = \beta = 0$, Jacobi-chaos becomes Legendre-chaos, and the first-order expansion is simply a uniform random variable. In this case, Gibb's oscillations are observed. As the values of (α, β) increase, the approximations improve. The expansion coefficients at different orders are tabulated in Table CI, together with the errors in variance and kurtosis compared with the 'exact' Gaussian distribution. It is seen that with $\alpha = \beta = 10$, even the first-order approximation, which is simply a beta random variable, has error in variance as little as 0.1%. The errors in kurtosis are larger because the Jacobi-chaos approximations do not possess tails. This, however, is exactly our objective.

REFERENCES

1. Lorentz J. Nonlinear singular perturbation problems and the Engquist–Osher difference scheme. *Technical Report 8115*, University of Nijmegen, Nijmegen, The Netherlands, 1981.
2. Kreiss G, Kreiss H-O. Convergence to steady state of solution of Burgers' equation. *Applied Numerical Mathematics* 1986; **2**:161–179.
3. Laforgue JGL, O'Malley RE Jr. On the motion of viscous shocks and the supersensitivity of their steady-state limits. *Methods in Applied Analysis* 1994; **1**:465–487.
4. Laforgue JGL, O'Malley RE Jr. Shock layer movement for Burgers' equation. *SIAM Journal on Applied Mathematics* 1994; **55**:332–347.
5. Laforgue JGL, O'Malley RE Jr. Viscous shock motion for advection-diffusion equations. *Studies in Applied Mathematics* 1995; **95**:147–170.
6. Laforgue JGL, O'Malley RE Jr. Exponential asymptotics, the viscous Burgers' equation, and standing wave solutions for a reaction-advection-diffusion model. *Studies in Applied Mathematics* 1999; **102**:137–172.
7. Reyna LG, Ward MJ. On exponential ill-conditioning and internal layer behavior. *Numerical Functional Analysis and Optimization* 1995; **16**:475–500.
8. Reyna LG, Ward WJ. On exponential slow motion of a viscous shock. *Communications on Pure and Applied Mathematics* 1995; **48**:79–120.
9. Garbey M, Kaper HA. Asymptotic-numerical study of supersensitivity for generalized Burgers' equations. *SIAM Journal of Scientific Computation* 2000; **22**:368–385.
10. Karniadakis GE, Sherwin SJ. *Spectral/hp Element Methods for CFD*. Oxford University Press: Oxford, 1999.
11. Xiu D, Karniadakis GE. Uncertainty modeling of Burgers' equation by generalized polynomial chaos. In *Computational Stochastic Mechanics. Proceedings of the Fourth International Conference on Computational Stochastic Mechanics*, Corfu, Greece, June 9–12, 2002, Spanos PD, Deodatis G (eds). Millpress: Rotterdam, 2003; 655–661.
12. Le Maitre O, Knio O, Najm H, Ghanem R. A stochastic projection method for fluid flow: basic formulation. *Journal of Computational Physics* 2001; **173**:481–511.
13. Le Maitre O, Reagan M, Najm H, Ghanem R, Knio O. A stochastic projection method for fluid flow: random process. *Journal of Computational Physics* 2002; **181**:9–44.
14. Xiu D, Karniadakis GE. Modeling uncertainty in flow simulations via generalized polynomial chaos. *Journal of Computational Physics* 2003; **187**:137–167.
15. Liu WK, Belytschko T, Mani A. Probabilistic finite elements for nonlinear structural dynamics. *Computer Methods in Applied Mechanics and Engineering* 1986; **56**:61–81.
16. Liu WK, Belytschko T, Mani A. Random field finite elements. *International Journal for Numerical Methods in Engineering* 1986; **23**:1831–1845.
17. Liu WK, Belytschko T, Mani A. Applications of probabilistic finite element methods in elastic/plastic dynamics. *Journal of Engineering for Industry* (ASME) 1987; **109**:2–8.
18. Kaminski M, Hien TD. Stochastic finite element modeling of transient heat transfer in layered composites. *International Communications in Heat and Mass Transfer* 1999; **26**(6):801–810.
19. Kleiber M, Hien TD. *The Stochastic Finite Element Method*. Wiley: New York, 1992.
20. Liu P-L, Der Kiureghian A. Finite element reliability of geometrically nonlinear uncertain structures. *Journal of Engineering and Mechanics* 1991; **117**:1806–1825.
21. Vanmarcke EH, Grigoriu M. Stochastic finite element analysis of simple beams. *Journal of Engineering and Mechanics* 1983; **109**:1203–1214.
22. Winter CL, Tartakovsky DM. Mean flow in composite porous media. *Geophysics Research Letters* 2000; **27**:1759–1762.
23. Winter CL, Tartakovsky DM. Groundwater flow in heterogeneous composite aquifers. *Water Resources Research* 2002; **38**:23.
24. Zhang D. *Stochastic Methods for Flow in Porous Media*. Academic Press: New York, 2002.
25. Zhu WQ, Wu WQ. A stochastic finite element method for real eigenvalue problems. *Probabilistic Engineering and Mechanics* 1991; **6**:228–232.
26. Xiu D, Karniadakis GE. The Wiener–Askey polynomial chaos for stochastic differential equations. *SIAM Journal on Scientific Computing* 2002; **24**(2):619–644.
27. Wiener N. The homogeneous chaos. *American Journal of Mathematics* 1938; **60**:897–936.
28. Ghanem RG. Scales of fluctuation and the propagation of uncertainty in random porous media. *Water Resources Research* 1998; **34**:2123.

29. Ghanem RG. Ingredients for a general purpose stochastic finite element formulation. *Computer Methods in Applied Mechanics and Engineering* 1999; **168**:19–34.
30. Ghanem RG, Brzakala W. Stochastic finite-element analysis of soil layers with random interface. *Journal of Engineering and Mechanics* (ASCE) 1996; **122**:361–369.
31. Ghanem RG, Red-Horse J. Propagation of uncertainty in complex physical systems using a stochastic finite elements approach. *Physica D* 1999; **133**:137–144.
32. Ghanem RG, Spanos P. *Stochastic Finite Elements: A Spectral Approach.* Springer: Berlin, 1991.
33. Chorin AJ. Hermite expansion in Monte-Carlo simulations. *Journal of Computational Physics* 1971; **8**: 472–482.
34. Chorin AJ. Gaussian fields and random flow. *Journal of Fluid Mechanics* 1974; **85**:325–347.
35. Crow SC, Canavan GH. Relationship between a Wiener–Hermite expansion and an energy cascade. *Journal of Fluid Mechanics* 1970; **41**:387–403.
36. Holden H, Oksendal B, Uboe OJ, Zhang T. *Stochastic Partial Differential Equations: A Modeling, White Noise Functional Approach.* Birkhäuser: Boston, 1996.
37. Matthies HG, Bucher C. Finite elements for stochastic media problems. *Computer Methods in Applied Mechanics and Engineering* 1999; **168**:3–17.
38. Orszag SA, Bissonnette LR. Dynamical properties of truncated Wiener–Hermite expansions. *Physics of Fluids* 1967; **10**:2603–2613.
39. Askey R, Wilson J. Some basic hypergeometric polynomials that generalize Jacobi polynomials. *Memoirs of the American Mathematical Society*. AMS: Providence RI, 1985; 319.
40. Schoutens W. *Stochastic Processes and Orthogonal Polynomials*. Springer: New York, 2000.
41. Xiu D, Karniadakis GE. Modeling uncertainty in steady state diffusion problems via generalized polynomial chaos. *Computer Methods in Applied Mechanics and Engineering* 2002; **191**:4927–4948.
42. Xiu D, Lucor D, Su C-H, Karniadakis GE. Stochastic modeling of flow-structure interactions using generalized polynomial chaos. *Journal of Fluids Engineering* 2002; **124**:51–59.
43. Xiu D. Generalized (Wiener-Askey) polynomial chaos, *Ph.D. Thesis*, Division of Applied Mathematics, Brown University, 2004.
44. Babuška I, Chatzipantelidis P. On solving elliptic stochastic partial differential equations. *Computer Methods in Applied Mechanics and Engineering* 2002; **191**:4093–4122.
45. Babuška I, Tempone R, Zouraris GE. Galerkin finite element approximations of stochastic elliptic differential equations. *Technical Report 02–38*, TICAM, 2002.
46. Deb MK, Babuška I, Oden JT. Solution of stochastic partial differential equations using Galerkin finite element techniques. *Computer Methods in Applied Mechanics and Engineering* 2001; **190**:6359–6372.
47. Glimm J. Nonlinear and stochastic phenomena: the grand challenge for partial differential equations. *SIAM Review* 1991; **33**:626–643.
48. Glimm J, Sharp DH. Prediction and the quantification of uncertainty. *Physica D* 1999; **133**:152–170.
49. Glimm J, Sharp DH. Stochastic partial differential equations: selected applications in continuum physics. In *Stochastic Partial Differential Equations: Six Perspectives*, Carmona RA, Rozovskii B (eds). American Mathematical Society: Providence, RI, 1999.
50. Huyse L, Walters RW. Random field solutions including boundary condition uncertainty for the steady-state generalized Burgers equation. *Technical Report 2001-35*, ICASE, 2001.
51. Walters RW, Huyse L. Uncertainty analysis for fluid mechanics with applications. *Technical Report 2002-1*, ICASE, 2002.
52. Murray JD. *Asymptotic Analysis*. Springer: New York, 1984.
53. Nafeh AH. *Perturbation Methods*. Wiley: New York, 1973.
54. O'Malley RE. *Introduction to Singular Perturbations*. Academic Press: New York, 1974.
55. Van Dyke M. *Perturbations Methods in Fluid Mechanics*. Panabolic Press: Stanford, 1975.
56. Xiu D, Karniadakis GE. A new stochastic approach to transient heat conduction modeling with uncertainty. *International Journal of Heat and Mass Transfer* 2003; **46**:4681–4693.

